

Sulfur chemistry and isotopic ratios in the starburst galaxy NGC 253

S. Martín

*Instituto de Radioastronomía Milimétrica (IRAM), Avda. Divina Pastora 7, Local 20,
E-18012 Granada, Spain*

J. Martín-Pintado

*Departamento de Astrofísica Molecular e Infrarroja, Instituto de Estructura de la Materia,
CSIC, Serrano 121, E-28006 Madrid, Spain*

R. Mauersberger

*Instituto de Radioastronomía Milimétrica (IRAM), Avda. Divina Pastora 7, Local 20,
E-18012 Granada, Spain*

C. Henkel

Max-Planck-Institut für Radioastronomie, Auf dem Hügel 69, D-53121 Bonn, Germany

S. García-Burillo

Observatorio de Madrid, Alfonso XII, 3, 28014 Madrid, Spain

ABSTRACT

Based on observations of the most abundant sulfur-bearing molecules (H_2S , CS, NS, SO, H_2CS , OCS, and SO_2) carried out with the IRAM 30m telescope ¹ and SEST ², we present the first analysis of the sulfur chemistry of an extragalactic source, the nuclear region of the starburst galaxy NGC 253. This is the first time that H_2S and, tentatively, H_2CS are detected towards the nucleus of a starburst galaxy. Source averaged fractional abundances of these molecules are a few 10^{-9} , except for CS and OCS which are more abundant (10^{-8}). Sulfur isotopic ratios, $^{32}\text{S}/^{34}\text{S} \sim 8 \pm 2$ and $^{34}\text{S}/^{33}\text{S} > 9$, are measured through observations of ^{13}CS ,

¹Based on observations carried out with the IRAM 30m telescope. IRAM is supported by INSU/CNRS (France), MPG (Germany) and IGN (Spain).

²Based on observations with the Swedish/ESO submillimetre telescope (SEST) at the European Southern Observatory, Chile. ESO N°70.B-0022.

$C^{34}S$, and $C^{33}S$. A comparison with the observed relative abundances towards different prototypical Galactic sources suggests that the chemical composition of NGC 253 is similar to that found towards the molecular clouds complexes like Sgr B2 in the nuclear region of the Milky Way. The large overabundance of OCS compared to the predictions of time-dependent sulfur chemistry models supports the idea that OCS is likely injected into the gas phase from the grain mantles by low velocity shocks.

Subject headings: galaxies: abundances — galaxies: active — galaxies: individual (NGC 253) — galaxies: ISM — galaxies: nuclei — galaxies: starburst

1. Introduction

The formation and evolution of stars strongly affects the chemistry of their molecular environment. In particular, sulfur-bearing molecules show enhanced abundances in the hot molecular cores, the condensations associated with massive protostars. The most accepted idea is that during the collapse of a star forming cloud, a large fraction of the available sulfur freezes out by accretion onto grain mantles and hydrogenates in the form of H_2S . The high temperatures and turbulent motions in these objects produced by the newly formed stars induce the evaporation and disruption of grain mantles, releasing the H_2S into the gas phase. After evaporation, this molecule is believed to drive a fast high temperature gas-phase chemistry leading first to the formation of SO and SO_2 and subsequently of other sulfur-bearing molecules such as CS and H_2CS (Charnley 1997; Hatchell et al. 1998). It is still uncertain whether the release of H_2S is caused exclusively by thermal evaporation or whether shocks play a role in the disruption of the grain mantles (Hatchell & Viti 2002). In low mass star-forming regions, where the temperatures are not high enough to evaporate the grain mantles, there is evidence that shocks may be responsible for injecting the H_2S from ices into the gas-phase (Buckle & Fuller 2003). Sulfur-bearing molecules are considered to be an important tool for studying the presence of shocks within massive star-forming regions. Time-dependent chemical models have roughly succeeded to reproduce the observed abundances of the most common sulfur-bearing species both in high and low mass star-forming regions (Hatchell et al. 1998; Buckle & Fuller 2003).

In starburst galaxies like NGC 253, only the most abundant sulfur-bearing molecules have been detected so far, namely CS, OCS, SO (Henkel & Bally 1985; Mauersberger et al. 1995; Petuchowski & Bennet 1992), and recently also SO_2 and NS (Martín et al. 2003). Extragalactic H_2S has only been detected toward the Large Magellanic Cloud, where H_2CS is also tentatively detected (Heikkilä et al. 1999). In this paper we present the first detection of

H₂S and the tentative detection of H₂CS in NGC 253, allowing us to investigate for the first time the sulfur chemistry in its nuclear region using a set of the most abundant sulfur-bearing species.

2. Observations

Most of the observations of the molecular species listed in Table 1 were carried out with the IRAM 30 m telescope on Pico Veleta (Spain). The measurements were made in symmetrical wobbler switching mode with a frequency of 0.5 Hz and a beamthrow of 4' in azimuth. As spectrometers, we used two 256 × 4 MHz filterbanks for the transitions at 2 mm and two 512 × 1 MHz filterbanks for those at 3 mm. The $J = 2 - 1$ and $J = 5 - 4$ transitions of CS were measured with the 15 m Swedish-ESO Submillimetre Telescope (SEST) at La Silla (Chile). Observations were done in wide dual beam switch mode, with 11.8' beam throw in azimuth. Acousto Optical Spectrometers were used as backends with a resolution of 1.4 MHz. Beam sizes ranged from 29'' (at 85 GHz) to 12'' (at 196 GHz) for the 30m telescope and from 51'' (at 98 GHz) to 21'' (at 244 GHz) for the SEST. In both telescopes, receivers were tuned to single side band with an image band rejection larger than 10dB. The spectra were calibrated with a dual load system.

Fig. 1 shows the observed line profiles of CS and two of its isotopic substitutions (¹³CS and C³⁴S), H₂S, SO, H₂CS, and OCS, as well as the corresponding Gaussian fits.

3. Results

For most of the observed transitions, we identify two velocity components, which arise from molecular cloud complexes at two opposing sides of the nucleus (Mauersberger et al. 1996), located at $\sim 5''$ NE (the 180 km s⁻¹ component) and $\sim 5''$ SW (the 280 km s⁻¹ component) as revealed by interferometric maps (Peng et al. 1996; García-Burillo et al. 2000).

The derived parameters from the Gaussian fits to the observed profiles are shown in Table 1. While most of the transitions of the main isotopic species of CS have already been reported (Mauersberger & Henkel 1989; Henkel et al. 1993), the improved signal-to-noise ratios of our data allow us for the first time to separate the two main velocity components in the line profiles. Unfortunately, the 2 mm lines of H₂CS appear to be blended with other lines. The 4_{1,4} – 3_{1,3} transition is blended with the H36 α recombination line and the 4_{1,3} – 3_{1,2} transition is contaminated by a contribution of the CS $J = 3 - 2$ line from the image band. In order to perform the Gaussian fits to the H₂CS lines, we have respectively subtracted

a Gaussian profile similar to that observed for the H34 α line measured at 160 GHz and the CS $J = 3 - 2$ emission measured in the signal band corrected by the corresponding image gain. As seen in the lower panel of the H₂CS lines in Fig. 1, the CS and the H₂CS lines do not fully account for the observed feature. The extra emission could be due to the presence of another unidentified line. In spite of the uncertainties due to the blending, both resulting H₂CS profiles are self-consistent, since they are expected to have similar intensities. Nevertheless, this detection must be regarded as tentative. Similarly, the OCS $J = 7 - 6$ transition appears blended with the $J = 1 - 0$ line of HC¹⁸O⁺. Additional observation of the HC¹⁸O⁺ $J = 2 - 1$ transition at 170 GHz allowed us to estimate and subtract the contribution of this species to the observed feature, by assuming local thermodynamic equilibrium (LTE) with an excitation temperature $T_{\text{ex}} \sim 12$ K.

3.1. Molecular abundances and excitation temperatures

In order to derive the physical properties of the molecular material we need to make an assumption on the total emission extent of the molecular emitting region. By smoothing the interferometric CS data from Peng et al. (1996), Mauersberger et al. (2003) derived the dependence of the observed line intensity on the beam size. This dependence indicates an equivalent source size of $\sim 20''$ for the CS emitting region. The interferometer maps of CS only miss 36% of the flux (Peng et al. 1996) suggesting that the extent of the CS emission is not much larger than this estimate. As we have no additional information on the extent of the emission of the other rarer species, we will assume them to be similar to that of CS. This assumption is supported by the comparison of the high angular resolution maps of the CS emission with those of species with a fairly different chemistry such as SiO, H¹³CO⁺ (García-Burillo et al. 2000) and NH₃ (M. Lebron, private communication), where the morphology of the emission seems to be similar.

We have derived source averaged column densities by correcting the measured line intensities for the estimated source size of $20''$ assuming optically thin emission. The corresponding population diagrams for CS, SO, and OCS are shown in Fig. 2. For CS we show the population diagrams for the two velocity components at 180 and 280 km s⁻¹ and we derive a rotational temperature $T_{\text{rot}} \sim 10$ K for both components. In these diagrams, the population in the $J = 2$ level, clearly above the linear fit, shows evidence for the presence of a lower excitation temperature component with $T_{\text{rot}} \sim 5$ K which can be explained by the much larger region observed by the $51''$ beam of the SEST. As derived below, the CS emission is moderately optically thick. The effect of the opacity on the population diagram would result in a slight increase of the derived excitation temperatures. Thus we would get

temperatures of ~ 13 K and ~ 8 K for the two components. To derive the CS column density in Table 2 we have used the optically thin emission of one of its isotopes, ^{13}CS . For OCS we derive a $T_{\text{rot}} = 16$ K. Our estimate of the OCS column density in Table 2 is in agreement with that derived by Mauersberger et al. (1995) when the differences in the assumed source size are taken into account. For the 180 km s^{-1} component of SO we obtain a $T_{\text{rot}} = 23$ K. As seen in Fig. 2, the 280 km s^{-1} component of the SO $3_4 - 2_3$ transition ($E_u/k \sim 29$ K) has a higher intensity than expected if we assume, from the CS results, both components to have a similar rotational temperature (Fig. 2). This may be due to the contamination of this component by the emission feature observed at a velocity of $\sim 400 \text{ km s}^{-1}$ which we tentatively identify as the $8_{1,8} - 7_{1,7}$ transition of NH_2CN (Cyanamide). The measured integrated intensity has been then considered as an upper limit as shown in Fig. 2. We have therefore assumed a similar excitation temperature of 23 K for both velocity components to compute the column density of the 280 km s^{-1} component of SO. Since we have only one transition for H_2S and the two observed lines of H_2CS have the same upper level energy, we need to make an assumption on the excitation temperature of these species. As the Einstein coefficients of these transitions are similar to those of CS and SO_2 , we will take an excitation temperature of 12 K for both species according to that derived from CS in this work, and from SO_2 by Martín et al. (2003).

Table 2 shows the derived source averaged column densities, rotational temperatures and fractional abundances relative to H_2 for all the sulfur bearing molecules detected towards the nucleus of NGC 253. The main sources of uncertainty in the derived abundances are those from the assumed extent of the emitting region and the H_2 column density, which are assumed to be the same for all the species. Assuming the extreme case in which the molecular emission is confined to a much smaller region of $\sim 10''$ the derived source averaged column densities will be larger by less than a factor 2. However, these uncertainties are expected to be even smaller when column density ratios between different species are considered. A similar argument also applies to the uncertainties in the derived fractional abundances introduced by the assumed H_2 column density if, as already discussed, the spatial distribution among different species does not vary substantially. Since we will focus our discussion on the molecular abundance ratios between different species, these uncertainties will not affect our conclusions.

Given that the $J = 3 - 2$ transition of CS, ^{13}CS , and C^{34}S were observed with the same telescope we can compare the observed ^{12}CS to ^{13}CS line intensity ratio of 21 ± 3 with the $^{12}\text{C}/^{13}\text{C}$ ratio of 40 ± 10 estimated by Henkel et al. (1993). Assuming that the $^{12}\text{CS}/^{13}\text{CS}$ intensity ratio reflects the $^{12}\text{C}/^{13}\text{C}$ abundance ratio, we derive an optical depth for the ^{12}CS $J = 3 - 2$ transition of ~ 1.4 . Therefore from the measured $^{13}\text{CS}/\text{C}^{34}\text{S}$ line intensities and the $^{12}\text{C}/^{13}\text{C}$ ratio mentioned above we derive a $^{32}\text{S}/^{34}\text{S}$ abundance ratio of

8 ± 2 . From our non detection of the $C^{33}S$ line, it is possible to give a 3σ lower limit to the $^{34}S/^{33}S$ ratio of 9.

The line intensities corrected for beam dilution of the four observed transitions of CS and the $J = 3 - 2$ lines of ^{13}CS and $C^{34}S$ have been compared with the results of model calculations for the excitation of CS in which the Large Velocity Gradient approximation has been used. A linewidth of 100 km s^{-1} and a kinetic temperature $T_{\text{kin}}=100 \text{ K}$ (similar to the rotational temperature of 100–142 K derived from NH_3 measurements by Mauersberger et al. (2003)) have been considered in these non-LTE calculations. Fig. 3 shows the results of this model for the observed line intensities and line ratios. The grey region corresponds to the best fit to the observed CS main isotope line intensities, calculated by minimizing the reduced χ^2 function as described by Nummelin et al. (2000). The best fit gives a CS column density $N(\text{CS})=5.7 \times 10^{13} \text{ cm}^{-2}$ and a molecular hydrogen density $n(\text{H}_2)=2.2 \times 10^5 \text{ cm}^{-3}$ for the velocity component at 180 km s^{-1} and $N(\text{CS})=5.7 \times 10^{13} \text{ cm}^{-2}$ and $n(\text{H}_2)=2.4 \times 10^5 \text{ cm}^{-3}$ for that at 280 km s^{-1} . These column densities are a factor of two lower than those in Table 2 derived from the isotopomer ^{13}CS assuming LTE conditions. The H_2 density derived from this analysis depends on the assumed kinetic temperature. Therefore, a T_{kin} of 50 K or 25 K would lead to H_2 densities a factor of 2 and 4 higher respectively. The choice of T_{kin} has, however, almost no effect on the column density determination.

As seen in Fig. 3 shows, the best fit contour does not cover the $J = 2 - 1$ data at a probability level of 99.5%. This fact suggests that the CS emission is best explained if one consider several gas components in the region covered by the telescope beam. These components are related to the need of two different excitation temperatures to fit the population diagram. The $J = 2 - 1$ to $1 - 0$ ratio of 1.5 derived by Paglione et al. (1995), also plotted in Fig 3, supports this scenario. For the 180 km s^{-1} velocity component (Fig. 3(a)) a higher density component ($n(\text{H}_2) \sim 4 \times 10^5 \text{ cm}^{-3}$) explains the $J_u = 5, 4, 3$ transitions, and a lower density component ($n(\text{H}_2) \sim 6 \times 10^4 \text{ cm}^{-3}$), with a 3 times higher column density, explains the lower J transitions. Similar results, within the errors, can be derived for the 280 km s^{-1} component.

From the non-LTE calculations we derive $C^{32}S/C^{34}S$ ratios of 4–9 and $^{12}CS/^{13}CS$ ratios of 22–35 for the 180 and 280 km s^{-1} velocity components respectively. The $^{12}CS/^{13}CS$ intensity ratio obtained for the 180 km s^{-1} component is half the $^{12}C/^{13}C$ ratio estimated by Henkel et al. (1993) while that obtained for the 280 km s^{-1} component is closer to their value. This may be explained by the fact that the ^{13}CS observation by Henkel et al. (1993) where made towards a position $\sim 6''$ closer to the emission peak of the 280 km s^{-1} component.

4. Discussion

4.1. Molecular fractional abundances

We find that most of the sulfur-bearing species detected towards the nuclear region of NGC 253 show similar fractional abundances of a few 10^{-9} (Table 2). Only CS and OCS have abundances a factor of ~ 5 higher. In order to understand the mechanism that dominates the chemistry in the nuclear environment of NGC 253 we summarize in Table 3 the fractional abundances of all the sulfur-bearing molecules detected towards this starburst galaxy and those observed towards selected Galactic sources (hot cores, Galactic center clouds, dark clouds, photodissociation regions (PDRs) and shocks driven by massive protostars) which are dominated by different kinds of chemistry. The abundance ratios discussed on this section are also shown in Table 3.

The SO_2 abundance in PDRs is much lower, by a factor of 40, than that found in NGC 253. Thus, abundance ratios such as $\text{H}_2\text{S}/\text{SO}_2$ and CS/SO_2 can be used to establish the role of photodissociation in the chemistry of NGC 253. Particularly instructive is the SO/SO_2 abundance ratio. $\text{SO}/\text{SO}_2 \sim 100$ towards PDRs is about two orders of magnitude larger than that in NGC 253 which suggests that photodissociation does not play a major role in the chemistry of its nuclear region.

A comparison with dark clouds shows a clearly lower abundance of OCS than that observed towards NGC 253. The OCS/SO ratio is 0.1 and 0.4 in L134N and TMC-1 respectively, while we measure ~ 4 in NGC 253. The abundance ratios of SO_2/SO and $\text{H}_2\text{S}/\text{SO}$ of ~ 0.2 and ~ 0.05 respectively measured towards these dark clouds are also much smaller than the corresponding ratios of ~ 1 observed towards NGC 253. Therefore, dark molecular clouds like L134N and TMC-1 do not seem to dominate the molecular composition near the nucleus of NGC 253.

Chemistry driven by high velocity shocks in molecular outflows also differs significantly from the chemistry found in NGC 253. The OCS/SO ratio measured towards these sources is two orders of magnitude smaller than that in NGC 253, while $\text{CS}/\text{H}_2\text{S}$ is three orders of magnitude lower. The large abundance of H_2S , as well as the low abundance of molecules such as CS, OCS, and H_2CS in local molecular outflows, is not observed in NGC 253.

As far as the hot cores are concerned, the molecular abundances vary significantly between Galactic sources. Different evolutionary states may account for these observed differences. As seen in Table 3 the abundance ratios in the Orion hot core mostly disagree with those in NGC 253. The relative abundances of most of the species towards SGR B2(N) are similar to what we find in NGC 253 except for the underabundance of H_2S and OCS

with respect to the other molecules. The ratio OCS/SO is almost two orders of magnitude lower in both hot cores than in NGC 253. In addition, the low rotational temperatures ($T_{\text{rot}} < 25\text{K}$) derived for all the sulfur-bearing species in NGC 253 suggest that the observed emission cannot be due to hot cores where much higher rotational temperatures are expected ($T_{\text{kin}} > 70\text{K}$).

Martín et al. (2003) pointed out that the molecular abundances of SO₂, NO, and NS are similar to those found in the envelope of the SGR B2 molecular complex. Table 3 also includes the comparison with two different clouds in the envelope of SGR B2. The first position, labeled SGR B2(OH), is located 30" south of SGR B2 M, and the second one 100" north-east of SGR B2 M. SO₂, SO, and H₂CS abundances in the Galactic center clouds agree well with those observed towards NGC 253. OCS/SO abundances ratios of 5 and 9 are similar to the ratio of ~ 4 found in NGC 253.

Our study of the sulfur chemistry towards the nuclear region of NGC 253 seems to indicate a chemistry similar to that of the envelope of SGR B2 where low velocity shocks are thought to be the main heating mechanism of the molecular material (Flower et al. 1995; Martín-Pintado et al. 1997, 2001). The low rotational temperatures derived for NGC 253 are also in agreement with those derived by Cummins et al. (1986) in the SGR B2 envelope. These results support the idea of large scale low velocity shocks driving the chemistry of the inner molecular material in the nucleus of NGC 253 which is consistent with the high rotational temperatures derived from NH₃ and the large observed SiO abundances (García-Burillo et al. 2000; Mauersberger et al. 2003).

4.2. Chemical models

In order to get an insight into the dominant chemistry around the central region of NGC 253, we compare our results with those available from chemical models (Millar et al. 1997; Charnley 1997; Hatchell et al. 1998; Buckle & Fuller 2003). For this we will assume that the whole nuclear region of NGC 253 can be described as a single molecular cloud. This is not likely as we are observing a 200 pc region where a number of unresolved molecular complexes with different physical and chemical properties coexist. Nevertheless, the dominant observed chemistry in the nuclear region of NGC 253 could be characterized by a single giant cloud as observed for the envelope of SGR B2 which has a size of ~ 30 pc. The SiO mapping of the Galactic center region show molecular cloud complexes extended over even larger scales (Martín-Pintado et al. 1997).

We have compared the observed molecular abundances in NGC 253 with the time-

dependent models used by Hatchell et al. (1998) and Buckle & Fuller (2003) to describe the chemistry of hot cores and low mass protostars respectively. These models assume the release of H₂S from grain mantles as the main precursor of the sulfur chemistry. Models with $T_{\text{kin}} \leq 50$ K and $n(\text{H}_2) < 10^5 \text{cm}^{-3}$ seem to best reproduce the abundances measured for SO₂, SO, H₂S, and H₂CS shown in Table 3. This result is in agreement with the idea that the emission from the nuclear region of NGC 253 is dominated by low excitation temperature and moderately dense molecular clouds similar to those found in the Galactic center clouds.

However current chemical models fall short of accounting for the observed abundances of OCS by more than one order of magnitude. It has been pointed out by Hatchell et al. (1998) and van der Tak et al. (2003) that OCS may play an important role in the chemistry of sulfur-bearing molecules. Near-IR observations of massive protostars (Geballe et al. 1985; Tielens 1989; Palumbo et al. 1995) show that sulfur may freeze out onto grains not only in the form of H₂S but also in the form of OCS. In fact OCS is the only sulfur bearing molecule detected so far in icy grain mantles. This would imply that OCS is also sputtered from grains by shocks. Hatchell et al. (1998) revised the chemical model by including an initial large abundance of OCS as well as reducing that of H₂S, assuming these species are initially injected into the gas phase. These models, depending on the initially injected H₂S and OCS (Wakelam et al. 2004), may account for the high OCS abundance observed in the nuclear region of NGC 253.

4.3. Sulfur isotopic ratios

The ³²S/³⁴S abundance ratios of 8 ± 2 and 13.5 ± 2.5 observed towards the nuclear starburst environment of NGC 253 (Sect. 3) and NGC 4945 (Wang et al. 2004) respectively are similar to those found within the Galactic inner 3 kpc region, but considerably lower than the value of ~ 24 measured in the Galactic disk (Chin et al. 1996). The estimated lower limit of the ³⁴S/³³S ratio towards NGC 253 is higher than the abundance of ~ 6 measured towards most of the Galactic sources studied by Chin et al. (1996).

Massive stars, as well as type Ib/c and II supernovae, appear to slightly overproduce ³⁴S and underproduce ³³S compared to ³²S (see Chin et al. 1996, and references therein). Thus, the compact stellar clusters observed near the center of NGC 253 (Watson et al. 1996) and the estimated overall star formation rate of $3.6 \text{M}_{\odot} \text{yr}^{-1}$ (Strickland et al. 2004) and supernova rate (SNr) of $0.05\text{--}0.3 \text{yr}^{-1}$ (Mattila & Meikle 2001; Ulvestad & Antonucci 1997) might account for the low ³²S/³⁴S as well as the enhanced ³⁴S/³³S ratios in NGC 253. This fact is supported by the high massive star formation rate of $\sim 0.1 \text{M}_{\odot} \text{yr}^{-1}$ estimated by Forbes et al. (1993) for the inner 6'' of this starburst.

Uncertainties are large enough that the $^{32}\text{S}/^{34}\text{S}$ ratio observed towards NGC 253 may not significantly differ from that in NGC 4945, where slightly higher star formation and supernova rates (Strickland et al. 2004) might also have induced an overproduction of ^{34}S in its nuclear region.

J.M.-P. has been partially supported by the Ministerio de Ciencia Y Tecnología with grant ESP2002-01627, AYA2002-10113E, AYA2003-0090 and ESP2004-00665. We wish to thank F.F.S. van der Tak for critical reading of the manuscript.

REFERENCES

- Buckle, J.V., & Fuller, G.A. 2003, *A&A*, 399, 567
- Charnley, S.B. 1997, *ApJ*, 481, 396
- Chin, Y.-N., Henkel, C., Whiteoak, J.B., Langer, N., & Churchwell, E.B. 1996, *A&A*, 305, 960
- Cummins, S.E., Linke R.A., & Thaddeus P. 1986, *ApJS*, 60, 819
- Flower, D.R., Pineau des Forêts, G., & Walmsley, C.M. 1995, *A&A*, 294, 815
- Forbes, D.A., Ward, M.J., Rotaciuc, V., Blietz, M., Genzel, R., Drapatz, S., van der Werf, P.P., & Krabbe, A. 1993, *ApJ*, 406, L11
- Geballe, T.R., Baas, F., Greenberg, J.M., & Schutte, W. 1985, *A&A*, 146, L6
- García-Burillo, S., Martín-Pintado, J., Fuente, A., & Neri, R. 2000, *A&A*, 355, 499
- Hatchell, J., Thompson, M.A., Millar, T.J., & Macdonald, G.H. 1998, *A&A*, 338, 713
- Hatchell, J., & Viti, S. 2002, *A&A*, 381, L33
- Henkel, C., & Bally, J. 1985, *A&A*, 150, L25
- Henkel, C., Mauersberger, R., Wiklind, T., Hüttemeister, S., Lemme, C., & Millar, T.J. 1993, *A&A*, 268, L17
- Heikkilä, A., Johansson, L. E. B., & Olofsson, H. 1999, *A&A*, 344, 817
- Jansen, D.J., Spaans, M., Hogerheijde, M.R., & van Dishoeck, E.F. 1995, *A&A*, 303, 541
- Martín, S., Mauersberger, R., Martín-Pintado, J., García-Burillo, S., & Henkel, C. 2003, *A&A*, 411, L465
- Martín, S., Martín-Pintado, J., Mauersberger, R., Requena, M.A., in preparation
- Martín-Pintado, J., de Vicente, P., Fuente, A., & Planesas, P. 1997, *ApJ*, 482, L45
- Martín-Pintado, J., Rizzo, J.R., de Vicente, P., Rodríguez-Fernández, N.J., Fuente, A. 2001, *ApJ*, 548, L65
- Mattila, S. & Meikle, W.P.S. 2001, *MNRAS*, 324, 325
- Mauersberger, R., & Henkel, C. 1989, *A&A*, 223, 79

- Mauersberger, R., Henkel, C., & Chin, Y.-N., 1995, *A&A*, 294, 23
- Mauersberger, R., Henkel, C., Wielebinski, R., Wiklind, T., & Reuter, H.-P. 1996, *A&A*, 305, 421
- Mauersberger, R., Henkel, C., Weiß, A., Peck, A.B., & Hagiwara, Y. 2003, *A&A*, 403, 561
- McGonagle, D., Irvine, W.M., & Ohishi, M. 1994, *ApJ*, 422, 621
- McGonagle, D., & Irvine, W.M. 1997, *ApJ*, 477, 711
- Millar, T.J., Macdonald, G.H., & Gibb, A.G. 1997, *A&A*, 325, 1163
- Minh, Y.C., Irvine, W.M., McGonagle, D., & Ziurys, L.M. 1990, *ApJ*, 360, 136
- Minh, Y.C., Ziurys, L.M., Irvine, W.M., & McGonagle, D. 1991, *ApJ*, 366, 192
- Nummelin A., Bergman P., Hjalmarsen Å., Friberg, P., Irvine, W. M., Millar, T. J., Ohishi, M., & Saito, S. 2000, *ApJS*, 128, 213
- Ohishi, M., Irvine, W. M., & Kaifu, N. 1992, in *IAU Symp. 150, Astrochemistry of Cosmic Phenomena*, ed. P.D. Singh (Dordrecht: Kluwer), 171
- Paglione, T. A. D., Jackson, J. M., Ishizuki, S., & Nguyen-Q-Rieu 1995, *AJ*, 109, 1716
- Palumbo, M.E., Tielens, A.G.G.M., & Tokunaga, A.T. 1995, *ApJ*, 449, 674
- Peng, R., Zhou, S., Whiteoak, J. B., Lo, K. Y., & Sutton, E. C. 1996, *ApJ*, 470, 821
- Petuchowski, S. J., & Bennett, C. L. 1992, *ApJ*, 391, 137
- Strickland, D. K., Heckman, T. M., Colbert, E. J. M., Hoopes, C. G., & Weaver, K. A. 2004, *ApJ*, 606, 829
- Sutton, E.C., Peng, R., Danchi, W.C., Jaminet, P.A., Sandell, G., & Russell, A.P.G. 1995, *ApJS*, 97, 455
- Tielens, A.G.G.M. 1989, in *IAU Symp. 135, Interstellar Dust*, ed. L.J. Allamandola & A.G.G.M. Tielens (Dordrecht: Kluwer), 239
- Ulvestad, J.S & Antonucci, R.R.J. 1997, *ApJ*, 488, 621
- van der Tak, F.F.S., Boonman, A.M.S., Braakman, R., & van Dishoeck, E.F. 2003, *A&A*, 412, 133

Wakelam, V., Caselli, P., Ceccarelli, C., Herbst, E. & Castets, A. 2004, *A&A*, 422, 159

Wang, M., Henkel, C., Chin, Y.-N., Whiteoak, J., Cunningham, M., Mauersberger, R., & Muders, D. 2004, *A&A*, 422, 883

Watson, A. M., et al. 1996, *AJ*, 112, 534

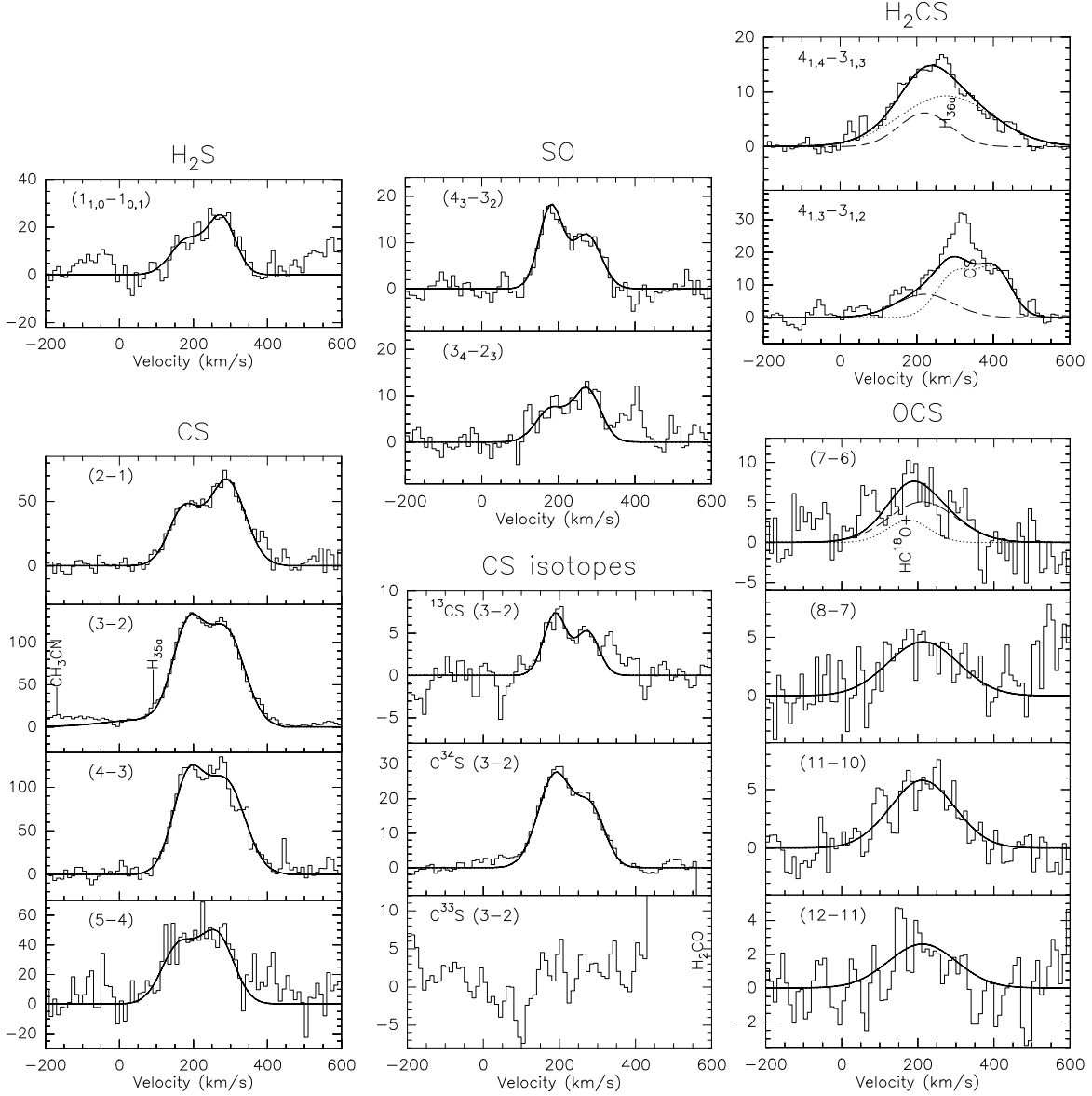


Fig. 1.— Gaussian fits to the detected transitions of H_2S , CS , ^{13}CS , C^{34}S , SO , H_2CS , and OCS towards the nuclear region of NGC 253 ($\alpha_{J2000} = 00^{\text{h}}47^{\text{m}}33^{\text{s}}.4$, $\delta_{J2000} = -25^{\circ}17'23''$). The velocity resolution has been smoothed to 10 km s^{-1} . Intensities are given in T_{MB} (mK). The figure for H_2CS shows in dashed lines the fits to the H_2CS transitions, in dotted lines the assumed $\text{H}36\alpha$ and CS profiles and in thick line the total fit. Similarly, the figure for the $\text{OCS } J = 7 - 6$ transition shows the calculated HC^{18}O^+ in dotted line.

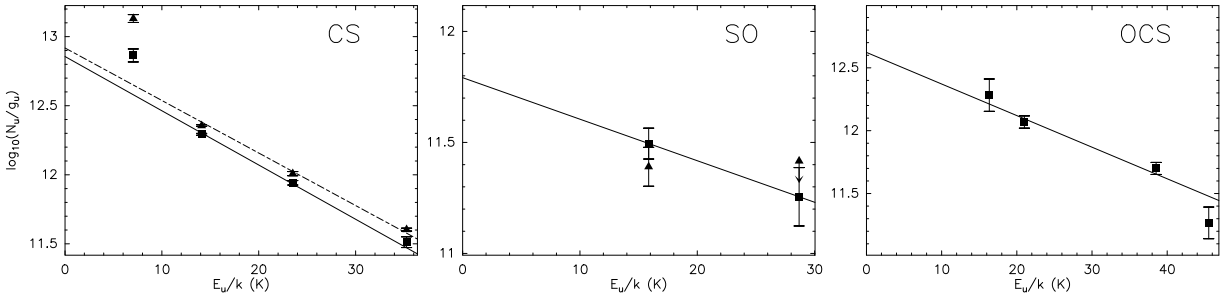


Fig. 2.— Population diagrams for the CS, SO, and OCS molecules. 180 km s⁻¹ component is represented by squares and continuous lines, the 280 km s⁻¹ component is shown with triangles and dashed lines.

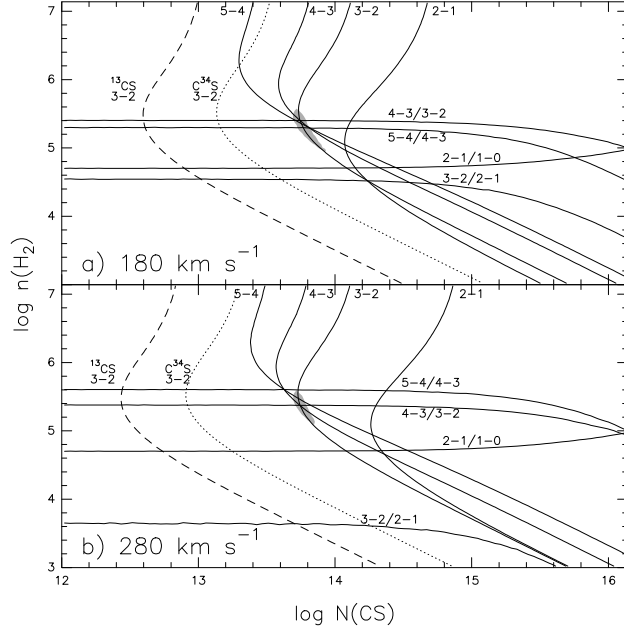


Fig. 3.— LVG model predictions for the observed CS transitions and for the $J = 3 - 2$ line of its isotopomers ^{13}CS and C^{34}S at a $T_{\text{kin}}=100\text{K}$ as a function of the H_2 density and the CS column density. Upper and lower pannel correspond to the 180 and 280 km s^{-1} velocity components respectively. Lines show the measured line intensities and intensity ratios. The $2-1/1-0$ ratio is from Paglione et al. (1995). Best fit to the line intensities of CS that minimizes the reduced χ^2 function is shown in grey and corresponds to the probability of 99.5% of enclosing the true parameters.

Table 1: Parameters derived from Gaussian fits to the observed features.

Molecule	ν (MHz)	Transition $J - J'$	$\int T_{\text{MB}} dv$ (mK km s ⁻¹)	v_{LSR} (km s ⁻¹)	$\Delta v_{1/2}$ (km s ⁻¹)	T_{MB} (mK)	rms ^b (mK)			
H ₂ S	168762.8	1 _{1,0} – 1 _{0,1}	1520 (180)	180	100	14.3	4.7			
			2250 (80)	275	88	23.9				
CS	97981.0	2 – 1	4400 (500)	172	96	43.4	5.2			
			8200 (500)	290	116	66.5				
	146969.0	3 – 2	11900 (200)	185	100	111.2	4.1			
			13700 (200)	288	117	110.3				
	195954.2	4 – 3	11500 (400)	185 ^a	100	108.2	7.0			
			13400 (500)	288 ^a	121	104.5				
	244935.6	5 – 4	4400 (400)	158	107	38.2	10.8			
			5400 (130)	262	108	46.7				
C ³⁴ S	144617.1	3 – 2	3000 (300)	188	105	27.1	1.4			
			1500 (300)	284	86	16.1				
¹³ CS	138739.3	3 – 2	550 (70)	188	70	7.4	1.9			
			390 (50)	274	70 ^a	5.2				
C ³³ S	145755.8	3 – 2	< 600	< 3.5	2.8			
SO	138178.6	4 ₃ – 3 ₂	1400 (200)	180	73	17.8	2.1			
			1100 (200)	274	88	11.6				
	158971.8	3 ₄ – 2 ₃	700 (200)	180 ^a	92	7.2	2.9			
			1000 (200)	274 ^a	84	11.4				
H ₂ CS	135297.8	4 _{1,4} – 3 _{1,3}	1040 (90)	221	158	6.2	1.4			
			139483.4	4 _{1,3} – 3 _{1,2}	1340 (150)	221		176	7.2	2.0
OCS	85139.1	7 – 6	1100 (300)	212 ^a	210 ^a	5.1	2.7			
			97301.2	8 – 7	1080 (120)	214		219	4.6	1.8
			133785.9	11 – 10	1220 (130)	212		200	5.8	1.3
			145946.8	12 – 11	580 (170)	212 ^a		210 ^a	2.6	1.4

^afixed parameter.

^brms values in T_{mb} and smoothed to a 10 km s⁻¹ channel width.

Table 2: Physical parameters derived for each species.

Molecule	N (10^{13}cm^{-2})	T_{rot} (K)	$[X]/[H_2]^a$ 10^{-9}
H ₂ S	(180 km/s) 2.4	12	1.4
	(270 km/s) 3.6	12	2.1
CS ^b	(180 km/s) 20	9.7(0.4)	12
	(280 km/s) 14	10 (0.2)	8.2
NS ^c	5	8(1)	3
SO	(180 km/s) 3	23(14)	2
	(270 km/s) 2.5	23	1.5
H ₂ CS	4.6	12	2.7
OCS	26	16(2)	15
SO ₂ ^c	7	14(9)	4

Note. — Column densities are source averaged values over a 20'' region.

^aAssumed $N(H_2) = 1.7 \cdot 10^{22} \text{cm}^{-2}$ from Mauersberger et al. (2003).

^bColumn density derived using the optically thin ¹³CS line and assuming a ratio ¹²C/¹³C=40 (Henkel et al. 1993).

^cfrom Martín et al. (2003).

Table 3: Relative abundances of S-bearing molecules in different environments.

Molecule	Hot Cores			Galactic center clouds		Dark clouds		PDRs	Outflows
	NGC 253	SGR B2 (N) ^(a)	Orion K-L ^(b)	SGR B2 (OH) ^(c)	Sgr B2 (envelope) ^(d)	L134N ^(e)	TMC-1 ^(e)	Orion Bar ^(f)	Orion Plateau ^(b)
H ₂ S	4	0.2 ^(g)	5000 ^(h)	...	1.5	0.8	<0.5	6	4000 ^(h)
CS	20	...	6	...	11	1	10	20	4
NS	3 ⁽ⁱ⁾	10	0.4 ^(j)	...	2.1	0.4 ^(k)	1 ^(k)
SO	4	20	190	4.4	6	20	5	9	200
H ₂ CS	3	20	0.8	6	5	0.6	3	...	8
OCS	15	2	11	21	53	2	2	...	10
SO ₂	4 ⁽ⁱ⁾	30	120	5.8	5.4	4	<1	0.1	100
H ₂ S/SO	1	0.01	26	...	0.25	0.04	<0.1	0.7	20
CS/SO ₂	5	...	0.005	...	2	0.25	<10	200	0.04
SO ₂ /SO	1	1.5	0.6	1.3	0.9	0.2	<0.2	0.01	0.5
OCS/SO	3.75	0.1	0.06	4.8	8.8	0.1	0.4	...	0.05
CS/H ₂ S	5	...	0.001	...	7.3	1.25	>20	3.3	0.001

Note. — Units of 10^{-9} are used.

References. — (a) Nummelin et al. (2000); (b) Sutton et al. (1995); (c) Cummins et al. (1986) assuming $N(\text{H}_2)=1 \times 10^{23}\text{cm}^{-2}$; (d) Martín et al. (in preparation); (e) Ohishi et al. (1992); (f) Jansen et al. (1995); (g) Minh et al. (1991); (h) Minh et al. (1990); (i) Martín et al. (2003); (j) McGonagle & Irvine (1997); (k) McGonagle et al. (1994);